DELPHI Collaboration

DELPHI 2003-024 CONF 644
8 June, 2003

Determination of the b quark mass at the M_Z scale with the DELPHI detector at LEP

P. Bambade
LAL, Orsay
M.J. Costa, J. Fuster and P. Tortosa
IFIC, València

Abstract

Measurements of the normalized three-jet rate of b quarks with respect to light ($\ell \equiv u, d, s$) quarks, $R_3^{b\ell}$, defined using the DURHAM and CAMBRIDGE jet algorithms, are described, using data collected by the DELPHI experiment at LEP on the Z peak from 1994 to 2000. They are used to extract values for the b quark mass at the M_Z energy scale defined in the $\overline{\rm MS}$ scheme, $m_b(M_Z)$, by comparing with next-to-leading order massive calculations and assuming α_s universality. The best determination:

$$m_b(M_Z) = 2.96^{+0.17}_{-0.18}\ (\text{stat}) \pm 0.19\ (\text{had}) \pm 0.14\ (\text{exp}) \pm 0.12\ (\text{theo})\ \text{GeV/c}^2,$$

obtained with CAMBRIDGE, has a total uncertainty of about ± 0.3 GeV/c^2. It is compatible with other direct determinations of the b quark mass at the M_Z energy scale and confirms the running predicted in QCD when compared with low energy determinations. The results presented update and supersede those already published using data collected from 1992 to 1994. The improved precision achieved results from the higher statistics used as well as from a better understanding of the hadronization process, flavour tagging and gluon splitting rates into heavy quarks. A new source of systematic uncertainty, related to the b mass parameter defined in the generator used to compute hadronization corrections, is found to be dominant, contributing about ± 0.15 GeV/c^2 to the final error. The results presented in this note are preliminary.

Contributed Paper for EPS 2003 (Aachen) and LP 2003 (FNAL)

1 Introduction

The b quark mass is a fundamental parameter in the Standard Model Lagrangian and therefore needs to be determined experimentally with the highest possible precision. However, confinement of quarks inside the observed hadrons introduces an additional complication with respect to lepton mass determinations. Quark masses need then to be defined within a theoretical convention and they can only be determined indirectly through their influence on hadron properties.

Among the different quark mass definitions, the most commonly used are the pole mass M_b and the running mass $m_b(Q)$. The former is defined as the pole of the renormalized quark propagator and it is gauge and scheme independent. The latter corresponds to the renormalized mass in the $\overline{\rm MS}$ scheme and therefore it is an energy scale and scheme dependent quantity. Both mass definitions are related to each other [1] and Next-to-leading order (NLO) calculations are needed in order to distinguish among the two. Physics should be independent on the mass definition used but at a fixed order in perturbation theory there is a dependence on the mass definition as well as on the arbitrary renormalization scale μ.

Determinations of the b quark mass have been performed at the production threshold and at the M_Z scale independently. At low energy, the b quark mass is inferred from the measured spectra of hadronic bound states or the moments of the B decay products spectra making use of nonperturbative techniques as Heavy Quark Effective Theory (HQET), Non-Relativistic QCD (NRQCD), lattice or QCD sum rules. An average of these determinations led to $m_b(m_b) = 4.24 \pm 0.11$ GeV/c^2 [2].

At the M_Z energy scale, the b quark mass was extracted from data collected at the Z^0 peak at LEP and SLC. At this high energy, b mass effects are negligible for inclusive observables since they are suppressed by $m_b^2/M_Z^2 \leq 0.3\%$. However, for more exclusive observables, like jet cross sections, they can be enhanced considerably for small enough values of the jet resolution parameter, y_c, as they go like $m_b^2/M_Z^2/y_c$ [3]. NLO calculations taking mass effects into account were performed for several event shape type observables and jet rates [4, 5, 6, 7], allowing determinations of the b quark mass at the M_Z energy scale [8, 9, 10, 11]. The results obtained for $m_b(M_Z)$ verify the scale evolution predicted by QCD when compared with the low energy determinations. However, the precision reached (which is $\sim 0.4 - 0.5$ GeV/c^2 at LEP) is lower than the one obtained at the production threshold (~ 0.1 GeV/c^2).

The first measurement of $m_b(M_Z)$ was performed by the DELPHI experiment with data collected from 1992 to 1994 at $\sqrt{s} \approx M_Z$. The observable used in this analysis was:

$$R_3^{b\ell} = \frac{\Gamma_{3j}^b(y_c)/\Gamma^b}{\Gamma_{3j}^\ell(y_c)/\Gamma^\ell} \tag{1}$$

being $\Gamma_{3j}^q(y_c)$ and Γ^q, respectively, the three-jet and total decay widths of the Z^0 into $q\overline{q}$, where $q = (b$ or $\ell \equiv uds$ quarks). The flavour q of the hadronic event was defined as that of the quarks coupled to the Z^0 and the DURHAM algorithm was used for jet clustering. The measured observable was compared with the theoretical computations of [4] and $m_b(M_Z)$ was found to be [8]:

$$m_b(M_Z) = 2.67 \pm 0.25 \text{ (stat)} \pm 0.34 \text{ (had)} \pm 0.27 \text{ (theo) GeV/c}^2 \tag{2}$$

which is dominated by hadronization uncertainties.

The motivation of the present analysis was to get a more precise determination of $m_b(M_Z)$ in order to test with high precision the predicted QCD energy scale evolution. Since most part of the running of m_b occurs up to M_Z, $m_b(M_Z)$ is a basic input parameter to constrain theories beyond the Standard Model as those predicting $m_b - m_\tau$ unification at the GUT scale. The running b quark mass has also important implications on Higgs searches since the partial decay width of the Higgs boson into b quarks is proportional to $m_b^2(m_H)$ in the Standard Model [12, 13, 14].

In this paper a new analysis to measure $m_b(M_Z)$ performed with data collected by DELPHI from 1994 to 2000 is presented. The same observable used in the previous DELPHI measurement, $R_3^{b\ell}$, has been used with two jet clustering algorithms, DURHAM and CAMBRIDGE. The CAMBRIDGE algorithm has the advantage of having a smaller theoretical uncertainty [7]. A detailed study of how mass effects and the hadronization process are implemented in the generators has led to a better control of the hadronization correction. The effect of the g splitting rates, $g \to b\overline{b}$ and $g \to c\overline{c}$, on the flavour tagging has also been taken into account.

2 The DELPHI detector

A brief description of the most relevant components of the DELPHI detector for this analysis is done here. A detailed description of its design and performance can be found in [15, 16].

DELPHI is an hermetic detector with a superconductive solenoid providing a uniform magnetic field of 1.23 T parallel to the beam axis throughout the central tracking device volume, allowing the determination of charged particles momentum with an average resolution of $\sigma(p)/p = 3.6\%$ for muons of 45 GeV/c.

The tracking system consists on a silicon Vertex Detector (VD), a jet chamber Inner Detector (ID), a Time Projection Chamber (TPC) which constitutes the main tracking device in DELPHI and a drift chamber Outer Detector (OD) covering the barrel region ($40^\circ \leq \theta \leq 140^\circ$) and two sets of drift chambers, FCA and FCB, located in the endcaps.

The VD, which is made of three coaxial cylindrical layers of silicon strip detectors, was upgraded in 1994 by instrumenting the outer and closer layers with doubled-sided orthogonal strips, allowing the measurement of both $R\phi$ and z coordinates. During 1991-1993 the VD provided measurements in the transverse plane only and that is why this set of data has been excluded in this analysis.

Electron and photon identification is provided mainly by the electromagnetic calorimeter which is composed by a High Density Projection Chamber (HPC) installed inside the coil in the barrel region and a lead-glass calorimeter (FEMC) in the forward region.

In order to measure the charged and neutral hadrons energy, DELPHI contains the hadron calorimetry (HCAL), an iron-glass sampling detector incorporated in the magnet yoke.

3 Experimental determination of $R_3^{b\ell}$

$R_3^{b\ell}$ can be measured at reconstruction level by applying the jet clustering algorithm (either DURHAM or CAMBRIDGE) to the samples of b and ℓ tagged events collected by DELPHI. However, the dependence of $R_3^{b\ell}$ with the b quark mass was calculated at NLO

with quarks and gluons instead of hadrons [4, 7]. Therefore, in order to compare the experimental result with the theoretical prediction the measured observable needs to be corrected for both detector (including acceptance and flavour tagging) and hadronization effects.

In the previous DELPHI measurement [8] it was shown that detector corrections are well determined while hadronization corrections are very sensitive to the different hadronization models used (the string model of PYTHIA or the HERWIG cluster model). We have shown that if a cut on b quark jet energy is done ($x_E^b(\text{jet}) = E_{b-\text{jet}}/E_{\text{beam}} \geq 0.55$) the two hadronization models lead to a similar hadronization correction and hence we restrict our measurement to this region of the phase space.

In this section the whole analysis procedure will be described, starting from the raw data and leading at the end to the $R_3^{b\ell}$ observable at hadron and parton level.

The first step was to select the sample of Z^0 hadronic decays, i.e. $Z^0 \to q\overline{q}$ events. From those events, the b and ℓ quark initiated events were separated using the DELPHI flavour tagging methods. In order to perform the cut on the b quark jet energies, a method to distinguish the b quark jets from the gluon jet was used based on the tagging of the quark flavour.

The jet clustering algorithms DURHAM and CAMBRIDGE were applied to both tagged samples to obtain the $R_3^{b\ell}$ observable at detector level. Data was then corrected for detector and tagging effects and the hadronization process to bring the observable to parton level.

3.1 Event selection

The selection of Z^0 hadronic events was done in three steps (as in [8]):

1. Particle selection: Charged and neutral particles reconstructed, respectively, in the tracking devices and in the calorimeters were selected in order to ensure a reliable determination of their momenta and energies by applying the cuts listed in Table 1.

2. Event selection: $Z^0 \to q\overline{q}$ events were selected by imposing the global event conditions of Table 1.

3. Kinematic selection: In order to reduce particle losses and wrong energy-momentum assignment to jets in the selected hadronic events, further kinematical cuts were applied. Each event was reconstructed to three jets by the jet clustering algorithm (DURHAM or CAMBRIDGE) using all charged and neutral selected particles, and the cuts of Table 2 were applied to each of them.

After applying all these cuts to the raw data a sample of 1.4×10^6 (1.3×10^6) hadronic Z^0 decays was selected for the DURHAM (CAMBRIDGE) algorithm.

3.2 Flavour tagging

Once the sample of Z^0 hadronic decays was selected, a method to distinguish between the b and $\ell \equiv uds$ quark initiated events had to be used.

DELPHI has developed two different algorithms for b tagging based on those properties of B hadrons that differ from those of other particles: the impact parameter [17] and the

Charged Particle Selection	$p \geq 0.1$ GeV/c $25^\circ \leq \theta \leq 155^\circ$ L$\geq$ 50 cm $d \leq 5$ cm in $R\phi$ plane $d \leq 10$ cm in z direction	
Neutral Cluster Selection	$E \geq 0.5$ GeV, $40^\circ \leq \theta \leq 140^\circ$ $E \geq 0.5$ GeV, $8^\circ(144^\circ) \leq \theta \leq 36^\circ(172^\circ)$ $E \geq 1$ GeV, $10^\circ \leq \theta \leq 170^\circ$	HPC FEMC HAC
Event Selection	$N_{ch} \geq 5$ $E_{ch} \geq 15$ GeV $\lvert\sum_i q_i\rvert \leq 6$, $i = 1, ..., N_{ch}$ No charged particle with $p \geq 40$ GeV/c $45^\circ \leq \theta_{thrust} \leq 135^\circ$	

Table 1: Particle and hadronic event selection; p is the particle momentum, θ the particle (and θ_{thrust} the $thrust$) polar angle with respect to the beam axis, L the measured track length, d the closest distance to the interaction point, q_i the particle charge, E the cluster energy, N_{ch} the number of charged particles, and E_{ch} the total charged particle energy in the event.

Kinematic Selection	$N_j^{ch} \geq 1$ per jet $E_j \geq 1$ GeV, $\quad j = 1, 2, 3$ $25^\circ \leq \theta_j \leq 155^\circ$, $\quad j = 1, 2, 3$ Planarity cut: $\sum_{ij} \phi_{ij} \geq 359^\circ$, $\quad i < j$, $\quad i, j = 1, 2, 3$

Table 2: Event selection based on the kinematic properties of the events when clustered in three jets by the jet algorithm. N_j^{ch} is the jet charged multiplicity, E_j the jet energy, θ_j the jet polar angle and ϕ_{ij} the angular separation between the pair of jets ij.

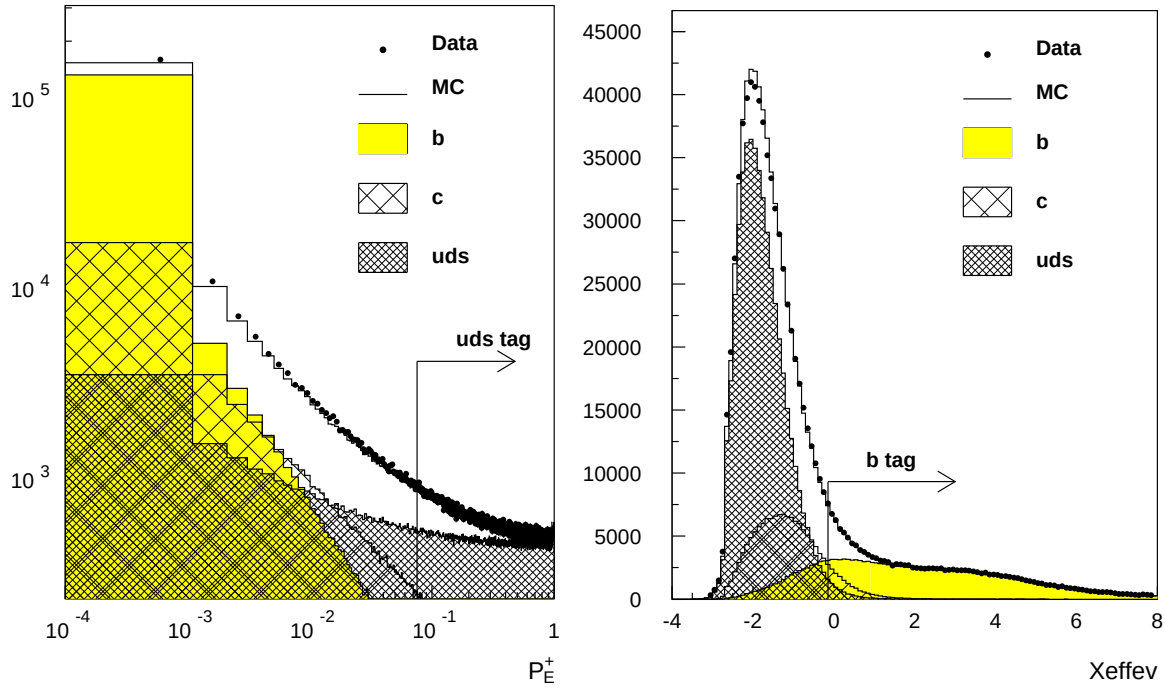

Figure 1: Event distribution of P_E^+ (left) and X_{effev} (right) when DURHAM is used to form jets. The real (points) and simulated (histogram) data are compared. The specific contribution of each quark flavour is displayed as derived from the DELPHI simulated data. The cuts used to tag the b and ℓ quark sample are also indicated.

combined technique [18]. The former makes use of the most important property for the selection of B hadrons, their long lifetime, and discriminates the flavour of the event by calculating the probability, P_E^+, of having all particles compatible with being generated in the event interaction point. For the second technique, an optimal combination of a set of discriminating variables defined for each reconstructed jet is performed, leading to a single variable per event, X_{effev}.

Figure 1 shows the distributions of P_E^+ and X_{effev} obtained for the selected real and simulated sample of Z^0 hadronic decays. For the case of the simulated data, the contribution of each quark flavour is also indicated.

Taking into account the stability of the final result (see Figure 2 left), the impact parameter method was used for ℓ tagging by imposing $P_E^+ > 0.07$ ($P_\ell = 82\%$, $\epsilon_\ell = 51\%$). For b tagging both techniques were observed to be equally stable and the combined method was used by requiring $X_{effev} > -0.15$ ($P_b = 86\%$, $\epsilon_b = 47\%$) because higher purities could be reached with the same efficiency.

In order to perform the cut on the b quark energies an identification of the gluon and b quark jets is required for b tagged events. The two tagging techniques can also provide a discriminative variable per jet and therefore both are available for jet identification. Again, based on a stability argument (see Figure 2 right), the combined technique was used to identify the pair of jets most likely to come from b quarks, with a jet purity of 81% and a cut efficiency of 90%.

Once the b quark jets were identified their energy was computed from the jet directions. Figure 3 shows the x_E^b(jet) distribution for real and simulated data. The cut $x_E^b(\text{jet}) \geq 0.55$

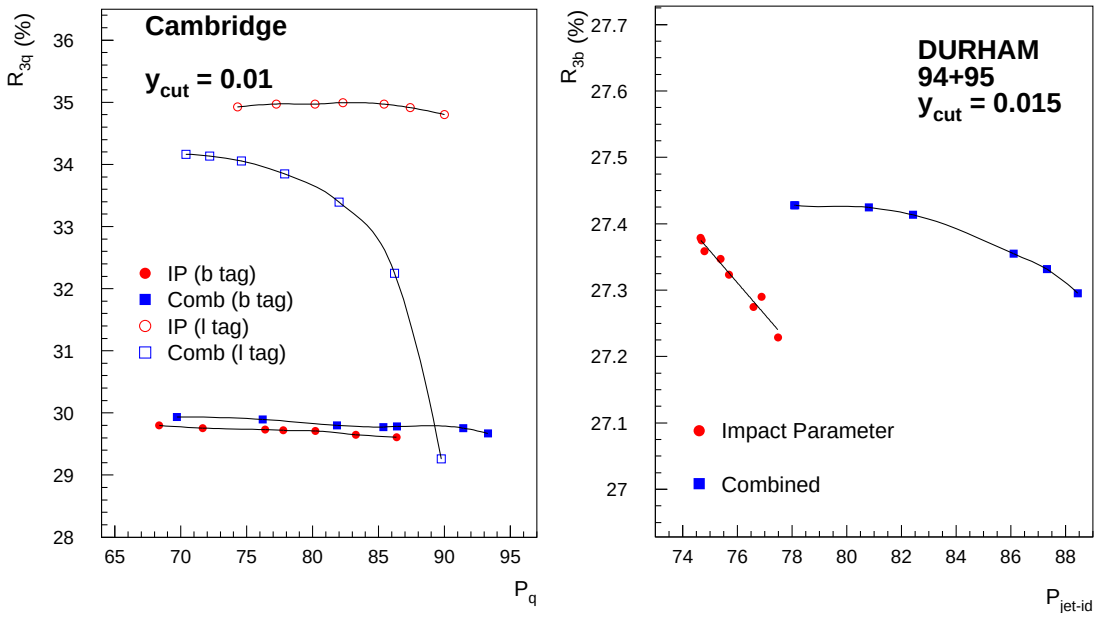

Figure 2: (Left) R_{3q} at parton level as a function of the purity of the q tagged sample, P_q, for $q = b, \ell$, when CAMBRIDGE is used to form jets. (Right) R_{3b} as a function of the jet identification purity at a $y_c = 0.015$ for the DURHAM algorithm.

was then applied for both b jets. The purity and contamination factors of the b and ℓ tagged samples obtained after the cut are shown in Table 3.

Method	Type q	$\ell \to q$ (%)	$c \to q$ (%)	$b \to q$ (%)
Impact Parameter	ℓ	82	15	3
Combined	b	2	7	91

Table 3: Flavour composition of the samples tagged as ℓ or b quark events.

3.3 Correction procedure

Once the b and ℓ quark hadronic events were selected from the collected data, the jet clustering algorithm was applied to get the $R_3^{b\ell}$ observable at detector level, $R_3^{b\ell-det}$. A correction procedure was then needed to bring the observable to parton level, $R_3^{b\ell-part}$, where a comparison with the theoretical calculations can be performed. The observable was corrected by detector, acceptance and tagging effects and the hadronization process using the following expression (which was derived in [8]),

$$R_3^{b\ell-part}(y_c) = \frac{\left[c_B^\ell g_{3B}^\ell(y_c) + c_B^c g_{3B}^c(y_c)\right] - \left[P_\ell g_{3L}^\ell(y_c) + c_L^c g_{3L}^c(y_c)\right] R_3^{b\ell-det}(y_c)}{c_L^b g_{3L}^b(y_c) R_3^{b\ell-det}(y_c) - P_b g_{3B}^b(y_c)} \qquad (3)$$

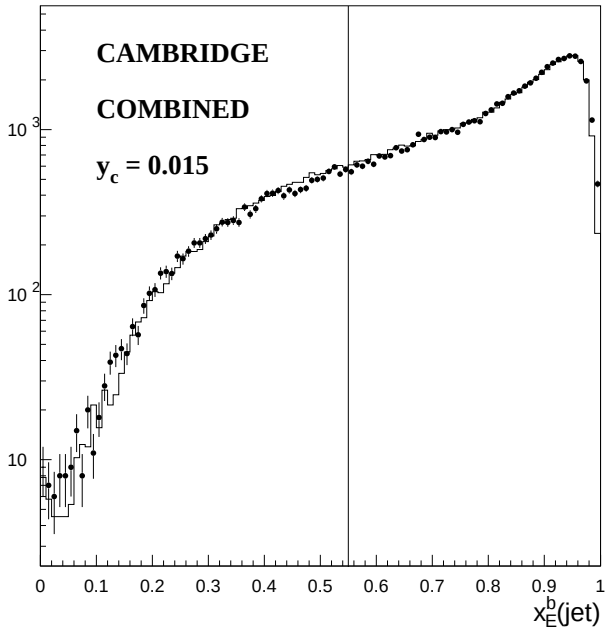

Figure 3: x_E^b(jet) distribution for real and DELSIM simulated data for three-jet b tagged events at a $y_c = 0.015$ for CAMBRIDGE.

where $g^i_{3Q}(y_c) = d^i_{3Q}(y_c) \cdot h_{3i}(y_c)$, being $d(y_c)$ the detector correction factors and $h(y_c)$ the hadronization ones,

$$d^i_{3Q}(y_c) = \frac{R^{i-det}_{3Q-MC}}{R^{i-had}_{3-MC}} \qquad h_{3i} = \frac{R^{i-had}_{3-MC}}{R^{i-part}_{3-MC}} \tag{4}$$

where $Q = B, L$ denotes, respectively, the b and ℓ tagged sample and $i = b, c, \ell$ refer to the real i-quark sample. Therefore, R^{i-det}_{3Q-MC} is the Monte Carlo three-jet rate at detector level of events that are tagged as Q and are of flavour i, R^{i-had}_{3-MC} is the three-jet rate at hadron level of the sample of i-quark events and R^{i-part}_{3-MC} the same rate but evaluated at parton level. The remaining factors of Eq. (3) correspond to the purities and contaminations of the two tagged samples listed in Table 3.

The complete DELPHI simulation (DELSIM), which uses JETSET 7.3 [19] to generate the events that go through the detector simulation, was used to compute the detector correction factors $d^i_{3Q}(y_c)$. A recent version of JETSET, PYTHIA 6.131 [20], tuned to DELPHI data [21], was used to get the hadronization factors.

The total size of the detector and hadronization corrections for $R_3^{b\ell}$ are shown in Figure 4. For instance, the detector correction is of about 2% for both algorithms while the fragmentation correction is about 5‰ for DURHAM and 1% for CAMBRIDGE at a $y_c = 0.02$ and $y_c = 0.01$ respectively.

Further corrections need to be applied to the $R_3^{b\ell}$ obtained by Eq. (3) in order to account for the correct heavy quark gluon splitting rates and a more reliable hadronization process in the simulated sample.

- **Gluon splitting rate correction**:

  In the present analysis, the flavour of the event was defined as that of the quarks directly coupled to the Z^0 boson and not from those quarks coming from secondary

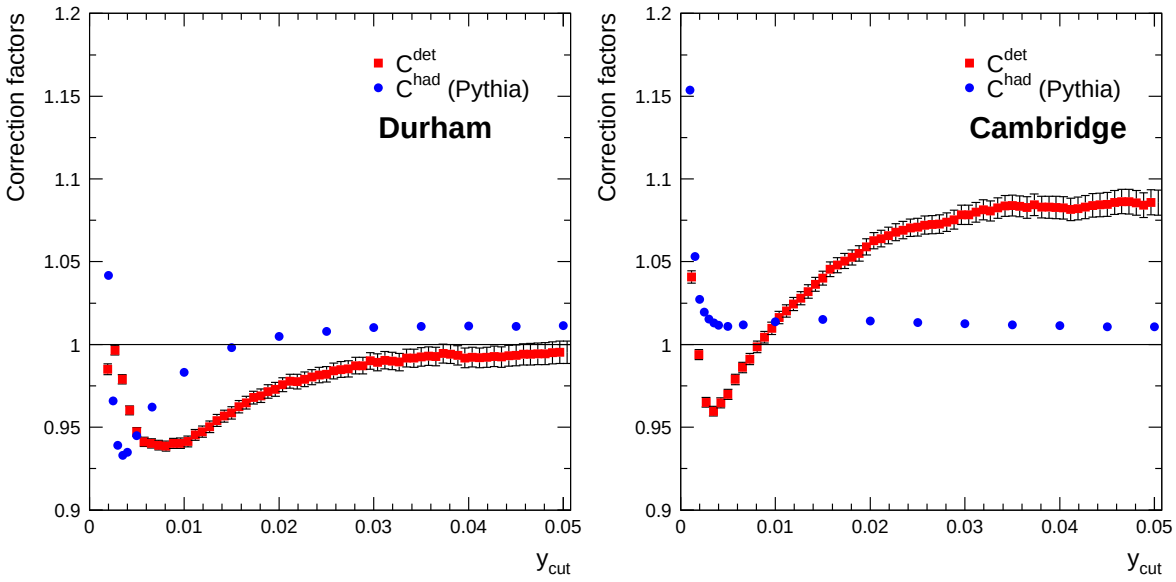

Figure 4: Detector and hadronization corrections applied to the measured $R_3^{b\ell}$ for DURHAM and CAMBRIDGE.

emissions due to gluon splitting processes. However, heavy quarks coming from $g \to b\overline{b}$ and $g \to c\overline{c}$ clearly affect the event tagging. Therefore, it is essential to have the correct gluon splitting rates, $g_{b\overline{b}}$ and $g_{c\overline{c}}$, in the simulated data used to correct the measured observable for detector and tagging effects. A reweighting of the DELSIM simulation was then done in order to have the measured rates [22]:

$$\begin{aligned} g_{c\overline{c}} &= 0.0296 \pm 0.0038 \\ g_{b\overline{b}} &= 0.00254 \pm 0.00051 \end{aligned} \tag{5}$$

which means a reweighting factor of 1.91 for events containing $g \to c\overline{c}$ processes and of 1.64 for those with $g \to b\overline{b}$. For instance, the impact of this reweighting on the measured observable is a reduction of $5‰$ at a $y_c = 0.02$ for the case of DURHAM and of $4‰$ at a $y_c = 0.01$ for CAMBRIDGE.

- **Additional hadronization corrections:**

  The hadronization correction factors used in the expression of Eq. (3) were computed with the PYTHIA generator using the same options than in the DELPHI tuning. This means that the string model was used for the hadronization process, the Peterson fragmentation function to fragment b quarks and a b mass of 5 GeV/c^2 was used in the perturbative phase. Two additional correction factors have been then applied to the $R_3^{b\ell-part}$ of Eq. (3) in order to correct for a more reliable hadronization process. These are:

  - **Model:**

    Three hadronization models were considered: the cluster one implemented in HERWIG [23], and two other models based on the string fragmentation of PYTHIA but with different heavy quark fragmentation functions, Peterson [24]

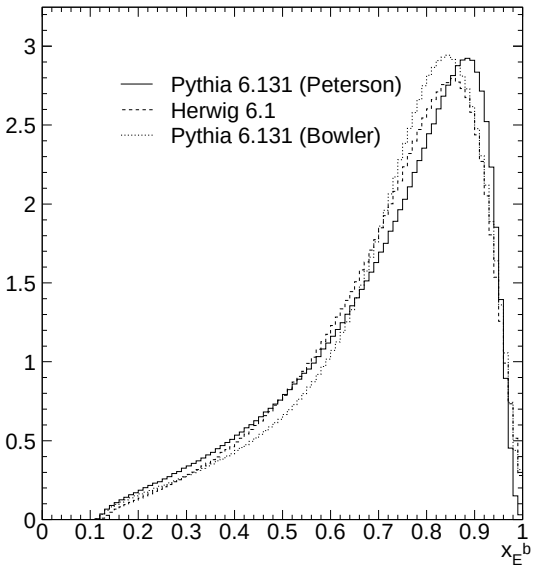

Figure 5: (x_E^b distribution for the different Monte Carlo generators, normalized to N_{ent}/N_{bin}, being N_{ent} and N_{bin} the number of entries and bins respectively.

and Bowler [25]. Figure 5 shows the b fragmentation function of the three models. The two generators used, PYTHIA 6.131 and HERWIG 6.1, were previously tuned to DELPHI data.

Since the three models describe the data reasonably well but the data does not prefer any of them [26], the mean of the three fragmentation corrections was used to correct the data.

– **b mass parameter in the generator**:

In order to describe mass effects, the PYTHIA generator uses three sets of quark masses, the kinematical, M_b, used at parton level, the constituent, M_b^{const}, used during the hadronization process and to derive B hadrons masses for states poorly or not measured, and the known B hadron masses. These three sets of masses are not connected to each other. Therefore, this situation is not appropriate to study mass effects because the changes made for parton masses don't propagate as they should during the hadronization process, resulting in hadronization corrections with an artificial dependence on the b quark mass value. If this connection is however imposed in the generator, this dependence can be removed, as was shown in [27].

It was also shown in [27] that the kinematical b quark mass used in PYTHIA at parton level can be identified as the pole mass within the uncertainty of the NLO theoretical calculations used to extract $m_b(M_Z)$ from $R_3^{b\ell}$. We then set the M_b parameter to a recent determination of the pole mass: 4.98 ± 0.13 GeV/c^2 [28].

Figure 6 shows for the two jet clustering algorithms the measured $R_3^{b\ell}$ at detector level and the one obtained at parton level after all the corrections were applied. The total correction is also shown in the plots, which is about 2% for both DURHAM and CAMBRIDGE at $y_c = 0.02$ and $y_c = 0.01$ respectively.

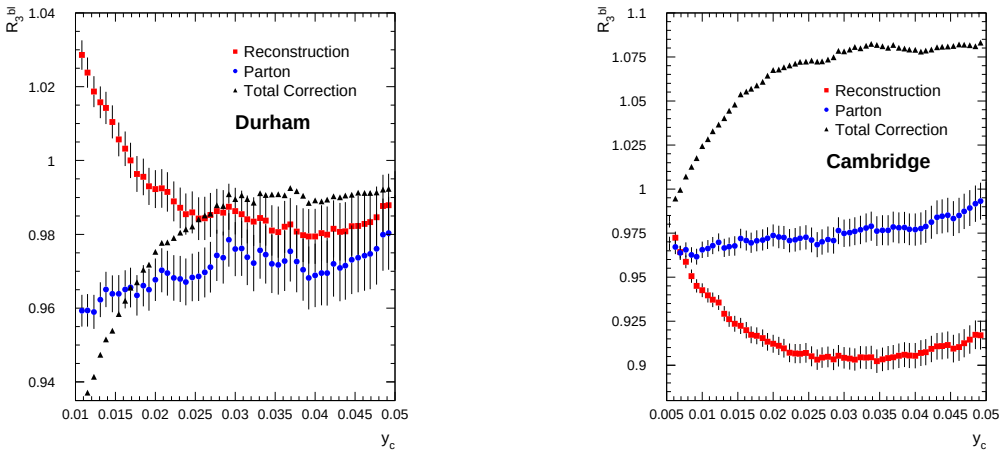

Figure 6: The measured $R_3^{b\ell}$ at detector level and parton level after all corrections, for the DURHAM (left) and CAMBRIDGE (right) algorithms. The total correction is also shown. The errors are only statistical.

3.4 Experimental uncertainties

Apart from the statistical uncertainties due to the limited size of the real and simulated data, different sources of systematic uncertainties were considered. They can be divided into two groups: those affecting the hadronization correction and the ones affecting the detector correction.

- **Hadronization**:

  The following contributions to the hadronization uncertainty have been taken into account:

  - **Tuning**: Uncertainty on the tuned parameters of PYTHIA that are relevant in the fragmentation process. This contribution was evaluated by varying these parameters ($\Lambda_{\rm QCD}$, Q_0, σ_q, ϵ_b, a) within $\pm\sigma$ from their central tuned values and taking into account that they are not completely independent [21].
  - **Hadronization model**: It was calculated as the standard deviation of the three hadronization corrections used. Figure 7 shows this uncertainty as a function of y_c for the present case in which a cut on x_E^b(jet) is done compared to the case in which no cut is made.
  - b **mass parameter ambiguity in the generator**: The uncertainty on the b mass parameter used in the generator, $M_b = 4.98 \pm 0.13$ GeV/c^2, was propagated to the effect on the hadronization correction.

- **Detector**:

  The uncertainties of the detector correction, which includes detector and acceptance effects and the tagging procedure, are due to imperfections on physics and detector modeling in the simulation. We have considered the following sources of uncertainties:

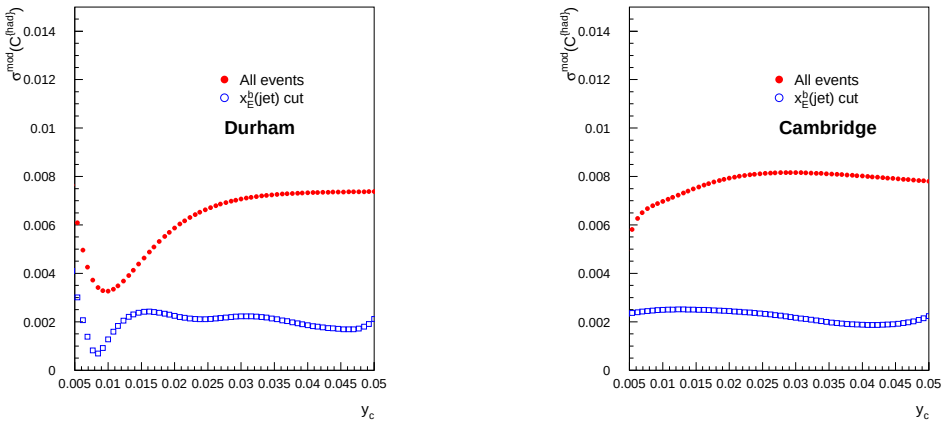

Figure 7: Hadronization model uncertainty as a function of the y_c for the DURHAM (left) and CAMBRIDGE (right).

- **Gluon splitting**: The gluon splitting rates of Eq. (6) were varied conservatively within twice their uncertainty and the effect on the measured observable was taken as the gluon splitting error.
- **Tagging**: It was evaluated by varying the purities and contamination factors of the correction formula of Eq. (3) within their uncertainty. The errors on P_b and P_ℓ were obtained from the known relative error of the b tagging and misstagging efficiencies, $\Delta\epsilon_B^b/\epsilon_B^b = 3\%$ and $\Delta\epsilon_B^\ell/\epsilon_B^\ell = \Delta\epsilon_B^c/\epsilon_B^c = 8\%$ [29], taking into account that ℓ tagging is just anti-b tagging, i.e. $\Delta\epsilon_L^q = \Delta\epsilon_B^q$ for $q = b, c, \ell$ for the same cut value.

  For each variation of the purities ($P_b = 91.2 \pm 1.0\%$ and $P_\ell = 82.3 \pm 1.6\%$) the contamination factors were varied accordingly using the closure relation $\sum_{q'=b,c,\ell} c_Q^{q'} = 1$ (where $c_Q^q \equiv P_q$) and keeping the factors c_B^ℓ/c_B^c and c_L^b/c_L^c constant.
- **Jet identification**: It was evaluated by varying the cut applied to distinguish the b quark jets from the gluon jet in a b tagged event within cut efficiencies of 80% to 100%. Half of the difference observed in the measured $R_3^{b\ell}$ at parton level is taken as the uncertainty due to the jet identification.

3.5 Results for $R_3^{b\ell}$ at parton and hadron level

The $R_3^{b\ell}$ obtained at parton level is shown in Figure 8 as a function of y_c together with its statistical and total uncertainties. The LO and NLO theoretical curves in terms of the pole and the running mass are also shown in the plot, for $M_b = 5$ GeV/c^2 and $m_b(M_Z) = 3$ GeV/c^2. The $R_3^{b\ell}$ values correspond to the average of the results obtained for each separate year since, as Figure 9 shows for a given y_c, all of them give compatible results. The measured $R_3^{b\ell}$ and its different experimental uncertainties are shown in Table 4.

$R_3^{b\ell}$ was also measured at hadron level by following the same correction procedure described in Section 3.3 but without correcting for the hadronization process. The purpose

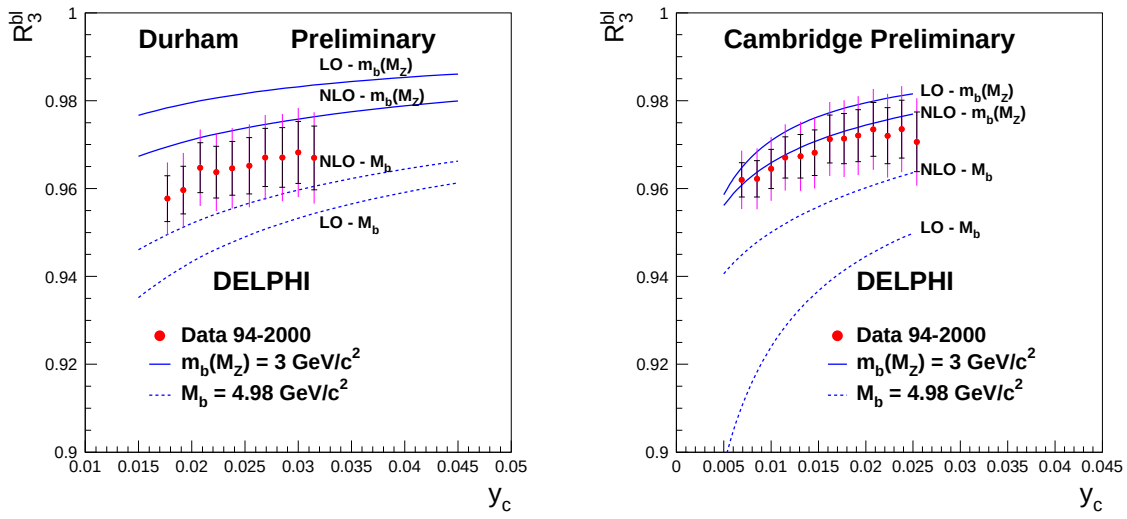

Figure 8: $R_3^{b\ell}$ as a function of y_c obtained at parton level compared with the LO and NLO theoretical predictions calculated in terms of a pole mass of $M_b = 4.98$ GeV/c^2 and in terms of a running mass of $m_b(M_Z) = 3$ GeV/c^2.

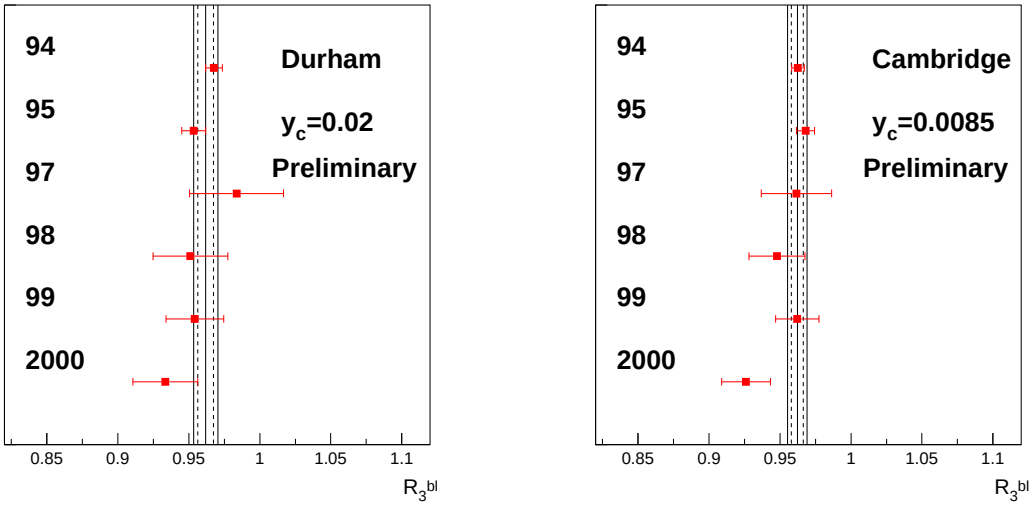

Figure 9: $R_3^{b\ell}$ at parton level obtained for each analysed year for a fixed y_c for DURHAM (left) and CAMBRIDGE (right). The error bars represent the statistical error. The vertical lines show the average value with its statistical and total error. The χ^2 per degree of freedom of the average is 0.7 and 1.2 for DURHAM and CAMBRIDGE respectively.

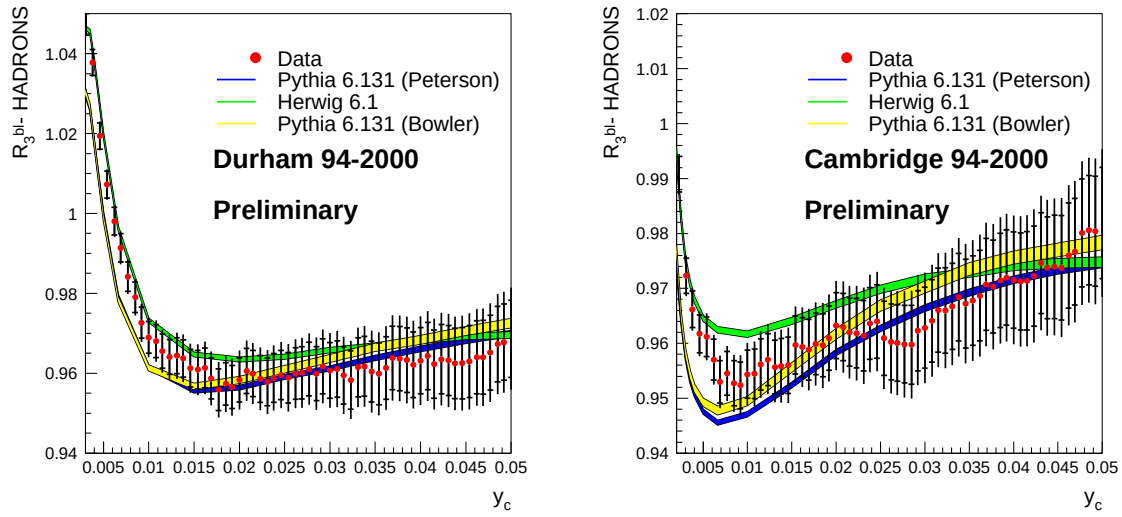

Figure 10: $R_3^{b\ell}$ at hadron level as a function of y_c compared with the PYTHIA 6.131 (with Peterson and Bowler fragmentation b functions) and HERWIG 6.1 predictions.

of this measurement was twofold: First, to compare with the prediction given by the PYTHIA and HERWIG generators and to study how well b mass effects are modeled. Second, a value at hadron level is useful in order to correct for other fragmentation models.

Figure 10 shows, as a function of the y_c, the measured $R_3^{b\ell}$ at hadron level together with the curves predicted by the two generators. For the case of PYTHIA, the curves are shown for the Peterson and Bowler b fragmentation functions. For large values of y_c, both generators describe well the data while, for small values, HERWIG gives a better prediction than PYTHIA, which tends to overestimate the mass effect.

4 Comparison with NLO massive calculations

The measurement of the $R_3^{b\ell}$ observable at parton level obtained in previous section, when compared with the NLO massive calculations of [4, 7], can be used to either extract the b quark mass assuming α_s universality or take as an input the b quark mass measured at threshold and extract the ratio of α_s for b and ℓ quark events.

In this section the results obtained with the two alternatives will be shown, although more emphasis will be put on the measurement of the b quark mass. For this case, both quark mass definitions, the running mass at the M_Z scale and the pole mass, will be derived from the measured observable.

4.1 Determination of the b quark mass

The theoretical predictions for $R_3^{b\ell}$ [4, 7] are written either in terms of the b quark pole or running mass which implies two different ways to get $m_b(M_Z)$ from the measured observable:

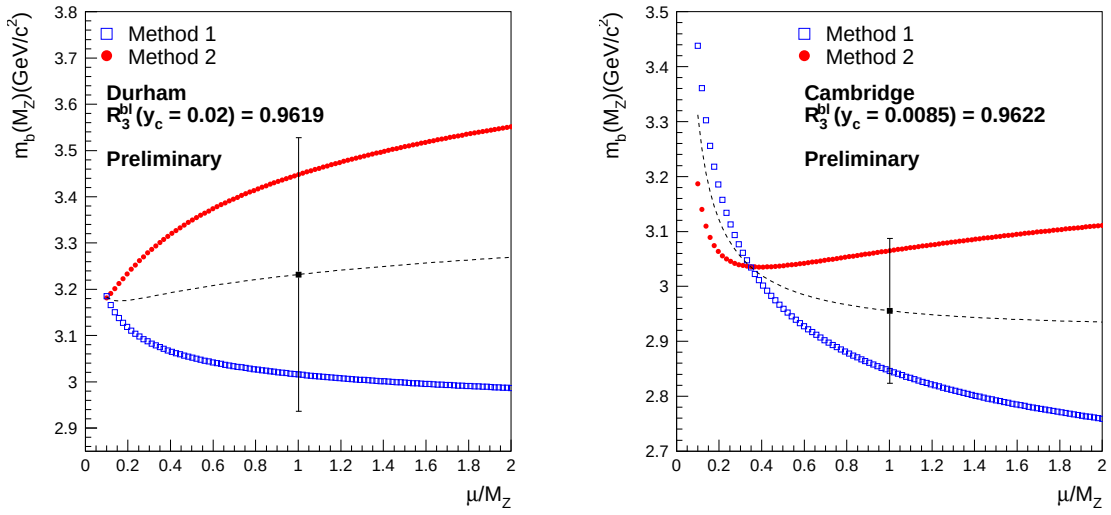

Figure 11: The extracted $m_b(M_Z)$ from the measured $R_3^{b\ell}$ as a function of the scale μ used, for DURHAM (left) and CAMBRIDGE (right). The result obtained for each method is shown, as well as the average of the two (dashed line). The result given at $\mu = M_Z$ is also displayed, where the error is just the theoretical one.

- Method 1: Use the parameterization in terms of the pole mass to extract a value for M_b, for an arbitrary value of μ. Then use the $\mathcal{O}(\alpha_s)$ relationship between M_b-$m_b(\mu)$ at $\mu = M_b$ to obtain $m_b(M_b)$ and the renormalization group equations (RGE) to go from $\mu = M_b$ to $\mu = M_Z$ to get $m_b(M_Z)$.

- Method 2: Use the expression in terms of the running mass to obtain, for an arbitrary scale μ, $m_b(\mu)$. Then use the RGE to evolve from that scale to M_Z to finally get $m_b(M_Z)$.

Figure 11 shows, for the measured value of $R_3^{b\ell}$ at a given y_c, the extracted $m_b(M_Z)$ for different values of μ. We have adopted the convention of giving the final result for $m_b(M_Z)$ as the mean of the results obtained by the two methods at $\mu = M_Z$ (as done in [8]). The theoretical uncertainty was estimated by considering the following sources:

- μ dependence: The μ scale was varied in the second method from $M_Z/2$ to $2M_Z$ and half of the difference of the result obtained on $m_b(M_Z)$ was taken as the μ scale error.

- Mass ambiguity: Half of the difference between the $m_b(M_Z)$ obtained for each method at $\mu = M_Z$ was taken as the error due to the mass ambiguity.

- α_s uncertainty: $\alpha_s(M_Z) = 0.1183 \pm 0.0027$ [30] was varied within its uncertainty and the effect on $m_b(M_Z)$ was taken as the error due to the uncertainty on α_s.

The b quark mass was extracted from the measured $R_3^{b\ell}$ at $y_c = 0.02$ and $y_c = 0.0085$ for DURHAM and CAMBRIDGE respectively. These jet resolution parameters were chosen

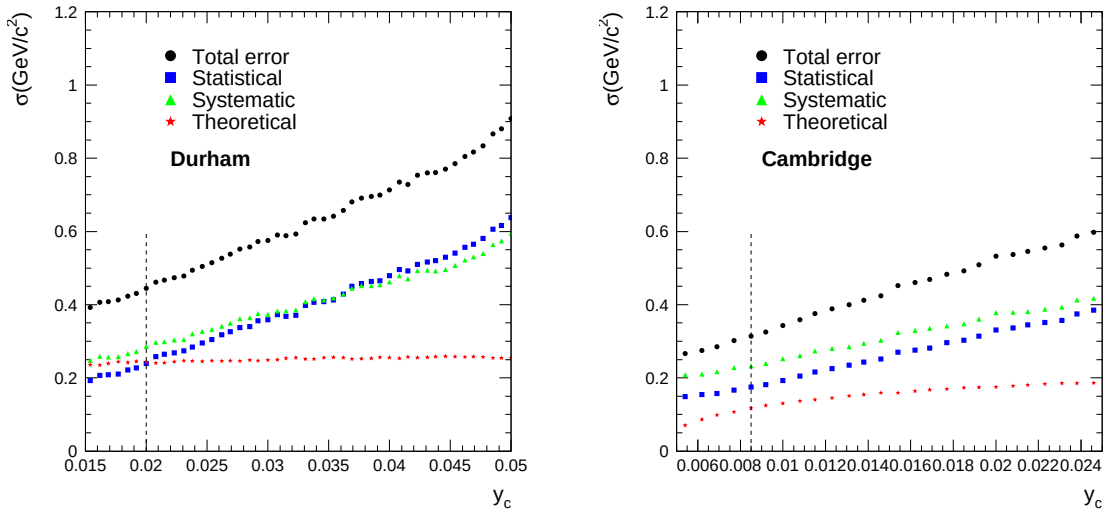

Figure 12: Total, statistical, systematic and theoretical uncertainty of $m_b(M_Z)$ as a function of y_c obtained from the measured values of $R_3^{b\ell}$ for DURHAM (left) and CAMBRIDGE (right). The vertical line represents the y_c value chosen to give the final $m_b(M_Z)$.

so to keep the hadronization correction, the total uncertainty and the four-jet rate small. As shown in Figure 4, the hadronization correction is constant for large values of y_c and it starts to decrease (increase) at $y_c = 0.015$ ($y_c = 0.005$) for DURHAM (CAMBRIDGE). In order not to be close to that region and to have the smallest uncertainty on the extracted $m_b(M_Z)$ (see Figure 12) these y_c values were selected.

The results obtained for $m_b(M_Z)$ are,

$$m_b(M_Z) = 3.23^{+0.24}_{-0.25}\ (\text{stat})^{+0.19}_{-0.20}\ (\text{had})^{+0.22}_{-0.23}\ (\text{exp}) \pm 0.24\ (\text{theo})\ \text{GeV/c}^2 \qquad (6)$$

when DURHAM is used to reconstruct jets and,

$$m_b(M_Z) = 2.96^{+0.17}_{-0.18}\ (\text{stat}) \pm 0.19\ (\text{had}) \pm 0.14\ (\text{exp}) \pm 0.12\ (\text{theo})\ \text{GeV/c}^2 \qquad (7)$$

when CAMBRIDGE is the algorithm used. The systematic uncertainties have been divided into the ones due to hadronization (had) and those due to the detector and physics modeling (exp). The contribution of each individual source of uncertainty is shown in Table 4.

The difference between the two results is smaller than the statistical error. The result obtained with CAMBRIDGE is more precise than the one obtained with DURHAM, mainly due to the reduction of the theoretical uncertainty, reaching a total error of $^{+0.31}_{-0.32}$ GeV/c^2 instead of $^{+0.45}_{-0.46}$ GeV/c^2.

Apart from the running mass, the b quark pole mass, M_b, can also be extracted from the measured $R_3^{b\ell}$ using the NLO expression of $R_3^{b\ell}$ in terms of the b pole mass. The theoretical uncertainty in this case was considered as the contribution of just the μ scale dependence and the α_s uncertainty, but no error was given due to the mass ambiguity. The μ scale was varied from $M_Z/10$ to $2M_Z$.

The measured b quark pole mass at $\mu = M_Z$ was found to be,

$$M_b = 4.48^{+0.30}_{-0.32}\ (\text{stat}) \pm 0.24\ (\text{had})^{+0.27}_{-0.29}\ (\text{exp}) \pm 0.13\ (\text{theo})\ \text{GeV/c}^2 \tag{8}$$

when DURHAM is used to reconstruct jets at $y_c = 0.02$ and,

$$M_b = 4.26^{+0.22}_{-0.23}\ (\text{stat})^{+0.24}_{-0.25}\ (\text{had})^{+0.17}_{-0.18}\ (\text{exp}) \pm 0.44\ (\text{theo})\ \text{GeV/c}^2 \tag{9}$$

when CAMBRIDGE is used instead at $y_c = 0.0085$. These values are low compared with the results obtained when the b pole mass is measured at low energy, as for example the one of [28] (4.98 ± 0.13 GeV/c^2), although they are compatible within errors. The theoretical uncertainty might be underestimated since no mass ambiguity has been considered.

4.2 Test of α_s flavour independence

The measurement of $R_3^{b\ell}$ can alternatively be used to test α_s flavour independence by using the relation introduced in [8]. Neglecting the $\mathcal{O}(\alpha_s)$ terms and taking as an input the average b quark mass from low energy measurements, $m_b(m_b) = 4.24 \pm 0.11$ GeV/c^2 [2], the ratio α_s^b/α_s^ℓ is found to be,

$$\alpha_s^b/\alpha_s^\ell = 0.989^{+0.006}_{-0.005}\ (\text{stat}) \pm 0.007\ (\text{syst}) \pm 0.005\ (\text{theo}) \tag{10}$$

for DURHAM and

$$\alpha_s^b/\alpha_s^\ell = 0.996 \pm 0.004\ (\text{stat}) \pm 0.006\ (\text{syst}) \pm 0.003\ (\text{theo}) \tag{11}$$

for CAMBRIDGE. These results verify α_s universality at a precision level of around 1%.

5 Conclusions

A new determination of the b quark mass at the M_Z scale has been performed with the DELPHI detector at LEP. The same observable as in the previous measurement [8] has been used but with jets reconstructed with two jet clustering algorithms, the already studied DURHAM and additionally CAMBRIDGE. The results obtained with CAMBRIDGE for $m_b(M_Z)$ were found to be more precise, mainly due to its better theoretical behaviour, reaching a total uncertainty of $^{+0.31}_{-0.32}$ GeV/c^2. This constitutes a substantial improvement with respect to the previous DELPHI measurement in which $m_b(M_Z)$ was determined with an uncertainty of ± 0.50 GeV/c^2.

The present measurement has been performed in a restricted region of the phase space to have a better control of the fragmentation process. The statistics was increased by analysing data collected at the Z^0 peak from 1994 until 2000. New versions of the generators, PYTHIA 6.131 and HERWIG 6.1, where mass effects are much better reproduced, have been used to correct the data.

The study performed in [27] of the way mass effects are implemented in the generators have led to a more reliable hadronization correction. The dependence of the hadronization correction on the b mass parameter set in the PYTHIA Monte Carlo was understood and quantified. It was shown that this effective mass parameter can be identified with the pole mass for the case of determining $m_b(M_Z)$ from $R_3^{b\ell}$. The uncertainty associated with

this parameter becomes the dominant source of error in the present result of $m_b(M_Z)$. It was also pointed out in [27] that this parameter could be constrained by fitting to the measured DELPHI data. However, the observable used for this fit was correlated with $R_3^{b\ell}$, and the corresponding determination was hence not used here. Further studies are being performed in order to find a more appropriate observable.

The effect of the $b\overline{b}$ and $c\overline{c}$ gluon splitting rates of the Monte Carlo on the detector correction has been taken into account. For the DURHAM algorithm, the correction and the error induced on the measurement by this effect are sizeable.

Figure 13 shows the result obtained by this analysis with CAMBRIDGE for $m_b(M_Z)$, together with the other LEP and SLC determinations. All these measurements are performed at the M_Z energy scale but for displaying reasons they are plotted at different scales. The data collected by DELPHI has also been used to determine the b quark mass at a lower energy scale from semileptonic B decays [31]. The value obtained using an unconstrained fit is also represented in this plot. In addition, the average of the results obtained when the b quark mass is measured at threshold [2], $M_\Upsilon/2$, is shown as well as the 3-loop running predicted by the RGE from this scale up to M_Z.

The result obtained in this analysis is compatible with the other measurements performed at the M_Z energy scale and it has the highest precision. It is also compatible with the low energy measurements (the average computed in [2] and the value obtained from DELPHI data [31]) taking into account the QCD energy evolution. A net change in the value of the running b quark mass between $\mu_1 = M_\Upsilon/2$ and $\mu_2 = M_Z$ is observed with about 3.5 standard deviations, $m_b(M_\Upsilon/2) - m_b(M_Z) = 1.20^{+0.34}_{-0.36}$ GeV/c^2, verifying the running of the b quark mass with the energy scale predicted by QCD. The b pole mass has also been extracted from the measured $R_3^{b\ell}$ and, although the value obtained is compatible with other determinations performed at the production threshold, it tends to be lower for both jet clustering algorithms.

Alternatively, universality of the strong coupling constant has also been verified with a precision of 8‰.

6 Acknowledgements

We are specially grateful to A. Santamaría and G. Rodrigo for providing the NLO massive calculations that made this measurement possible. We are also indebted to T. Sjöstrand for his help on understanding how mass effects are implemented in PYTHIA. We would also like to thank G. Dissertori for the continuous feedback and J. Portoles and M. Eidemüller for their information about the b pole mass. We are also pleased to thank the European network RTN2-2001-00450 for its support since this work has been developed as part of its activities.

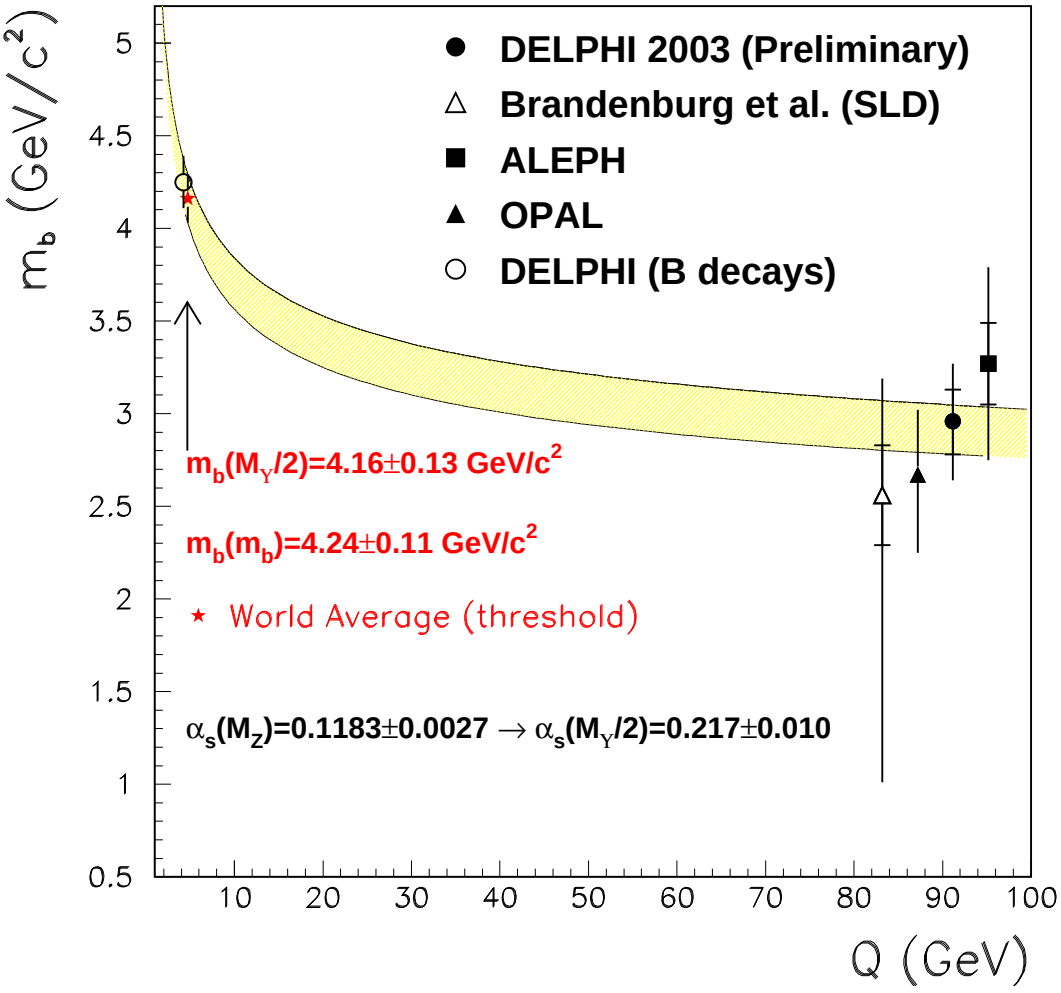

Figure 13: The running of $m_b(Q)$. The $m_b(M_Z)$ measured by LEP and SLC are displayed together with their total and statistical errors. The shaded area corresponds to the band associated to $m_b(Q)$ when running the average value obtained at $M_\Upsilon/2$ [2] up to the M_Z scale using the QCD renormalization group equations and $\alpha_s(M_Z) = 0.1183 \pm 0.0027$. The result obtained by DELPHI at low energy from semileptonic B decays [31] is also shown.

DURHAM (94-2000)	$R_3^{b\ell}(y_c = 0.02)$	$m_b(M_Z)$ GeV/c^2
Value	0.9619	3.23
Statistical Data	± 0.0045	$^{+0.20}_{-0.21}$
Statistical Simulation	± 0.0033	$^{+0.14}_{-0.15}$
Total statistical	± 0.0056	$^{+0.24}_{-0.25}$
Fragmentation Tuning	± 0.0015	± 0.07
Fragmentation Model	± 0.0022	± 0.10
Mass parameter	± 0.0034	± 0.15
Total hadronization	± 0.0042	$^{+0.19}_{-0.20}$
Gluon Splitting	± 0.0031	± 0.14
Tagging	$^{+0.0034}_{-0.0035}$	$^{+0.15}_{-0.16}$
Jet identification	± 0.0018	± 0.08
Total experimental	$^{+0.0049}_{-0.0050}$	$^{+0.22}_{-0.23}$
Mass Ambiguity	–	± 0.22
μ-scale ($0.5 \leq \mu/M_Z \leq 2$)	–	± 0.10
$\alpha_s(M_Z)$	–	± 0.03
Total theoretical		± 0.24
CAMBRIDGE (94-2000)	$R_3^{b\ell}(y_c = 0.0085)$	$m_b(M_Z)$ GeV/c^2
Value	0.9622	2.96
Statistical Data	± 0.0034	$^{+0.14}_{-0.15}$
Statistical Simulation	± 0.0024	± 0.10
Total statistical	± 0.0042	$^{+0.17}_{-0.18}$
Fragmentation Tuning	± 0.0010	± 0.04
Fragmentation Model	± 0.0025	± 0.11
Mass parameter	± 0.0036	$^{+0.15}_{-0.16}$
Total hadronization	± 0.0045	± 0.19
Gluon Splitting	± 0.0015	± 0.06
Tagging	± 0.0021	± 0.09
Jet identification	± 0.0020	± 0.09
Total experimental	± 0.0033	± 0.14
Mass Ambiguity	–	± 0.11
μ-scale ($0.5 \leq \mu/M_Z \leq 2$)	–	± 0.04
$\alpha_s(M_Z)$	–	± 0.01
Total theoretical		± 0.12

Table 4: Values of $R_3^{b\ell}$ and $m_b(M_Z)$ obtained with DURHAM and CAMBRIDGE algorithms and break-down of their associated errors (statistical and systematic) for $y_c = 0.02$ and $y_c = 0.0085$ respectively.

References

[1] R. Tarrach, Nucl. Phys. **B183** (1981) 384.

[2] A.X. El-Khadra, M. Luke, Ann. Rev. Nucl. Part. Sci. **52** (2002) 201.

[3] M. Bilenky, G. Rodrigo and A. Santamaría, Nucl. Phys. **B439** (1995) 505.

[4] G.Rodrigo, M. Bilenky, A. Santamaría, Phys. Rev. Lett. **79** (1997) 193.

[5] W.Bernreuther, A. Brandenburg, P. Uwer, Phys.Rev.Lett. **79** (1997) 189.

[6] P. Nason and C. Oleari, Phys. Lett. **B407** (1997) 57.

[7] M. Bilenky, S. Cabrera, J. Fuster, S. Martí, G. Rodrigo, A. Santamaría, Phys. Rev. **D60** (1999) 114006.

[8] DELPHI Coll., P.Abreu et al., Phys. Lett. **B418** (1998) 430-442;
S. Martí i García, J. Fuster and S. Cabrera, Nucl. Phys. **B** (Proc. Suppl.) **64** (1998) 376.

[9] A. Brandenburg, P.N. Burrows, D. Muller, N. Oishi, P. Uwer, Phys. Lett. **B468** (1999) 168.

[10] ALEPH Coll., R. Barate et al., Eur. Phys. Jour. **C18** (2000) 1.

[11] OPAL Coll., G. Abbiendi et al., Eur. Phys. J. **C21** (2001) 411.

[12] K.G. Chetyrkin and A. Kwiatkowski, Nucl. Phys. **B461** (1996) 3.

[13] K.G. Chetyrkin, B.A. Kniehl and M. Steinhauser, Phys. Rev. Lett. **79** (1997) 353.

[14] K.G. Chetyrkin and M. Steinhauser, Phys. Lett. **B408** (1997) 320.

[15] P. Aarnio et al., Nucl. Instr. and Meth. **A303** (1991) 233.

[16] DELPHI Coll., P. Abreu et al., Nucl. Instr. and Meth. **A378** (1996) 57.

[17] DELPHI Coll., P. Abreu et al., Z. Phys. **C65** (1995) 555;
G.V. Borisov, C. Mariotti, Nucl. Instr. and Meth. **A372** (1996) 181.

[18] G. Borisov, Nucl. Instr. and Meth. **A417** (1998) 384.

[19] T. Sjöstrand. Computer Physics Commun. **82** (1994) 74.

[20] T. Sjöstrand, P. Edén, C. Friberg, L. Lönnblad, G. Miu, S. Mrenna and E. Norrbin, Computer Physics Commun. **135** (2001) 238;
T. Sjöstrand, L. Lönnblad and S. Mrenna, *PYTHIA 6.2 Physics and Manual*, [hep-ph/0108264].

[21] DELPHI Coll., P. Abreu et al., Z. Phys. **C73** (1996) 11.

[22] The LEP/SLD Heavy Flavour Working Group, LEPHF/2001-01.

[23] G. Marchesini, B.R. Webber, G. Abbiendi, I.G. Knowles, M.H. Seymour and L. Stanco, Computer Phys. Commun. **67** (1992) 465;
G. Corcella, I.G. Knowles, G. Marchesini, S. Moretti, K. Odagiri, P. Richardson, M.H. Seymour and B.R. Webber, JHEP **0101** (2001) 010 [hep-ph/0011363]; [hep-ph/0201201].

[24] C. Peterson, D. Schlatter, I. Schmitt and P. Zerwas, Phys. Rev. **D27** (1983) 105.

[25] M.G. Bowler, Z. Phys. **C11** (1981) 168.

[26] SLD Coll., Kenji Abe et al., Phys. Rev. Lett. **84** (2000) 4300;
ALEPH Coll. Phys. Lett. **B512** (2001) 30;
OPAL Coll.,G. Abbiendi et al., Eur. Phys. J. **C13** (2000) 225;
DELPHI Coll., P. Abreu et al., Z. Phys. **C68** (1995) 353.

[27] P. Bambade, M.J. Costa, J. Fuster and P. Tortosa, DELPHI 2003-061-PHYS-932.

[28] M. Eidemüller, Phys. Rev. **D67** (2003) 113002.

[29] DELPHI Coll., P. Abreu et al., Eur. Phys. J. **C10** (1999) 415.

[30] S. Bethke, MPI-PhE-2002-17, [hep-ex/0211012].

[31] M. Battaglia et al., Phys. Lett. **B556** (2003) 41.